Submitted to small

Cross-linked g-C_3N_4/rGO nanocomposites with tunable band structure and enhanced visible light photocatalytic activity**

*Yibing Li, Haimin Zhang, Porun Liu, Dan Wang, Ying Li, and Huijun Zhao**

((Optional Dedication))

[*] Y. B. Li, Dr. H. M. Zhang, Dr. P. R. Liu, Prof .Y. Li, Prof. H. J. Zhao
Centre for Clean Environment and Energy
and Griffith School of Environment
Griffith University
Gold Coast Campus
Queensland 4222 (Australia)
E-mail: h.zhao@griffith.edu.au

Prof. D. Wang
State Key Laboratory of Multiphase Complex Systems
Institute of Process Engineering
Chinese Academy of Sciences
Beijing, 100190, (P. R. China)

Prof. Y. Li
School of Materials Science and Engineering
Shanghai University
Shanghai, 200072 (P. R. China)

Keywords: g-C_3N_4/reduced graphene oxide, Nanocomposite, Covalent bond, Band structure, Visible light photocatalysis

Cross-linked rather than non-covalently bonded g-C_3N_4/reduced graphene oxide (CN/rGO) nanocomposites with tunable band structure have been successfully fabricated by thermal treatment of a mixture of cyanamide and graphene oxide (GO) with different weight ratios. The experimental results indicate that compared to pure g-C_3N_4, the fabricated CN/rGO nanocomposites show narrowed bandgap with the increased rGO ratio in nanocomposites. Furthermore, the band structure of the CN/rGO nanocomposites can be readily tuned by simply controlling the weight ratio of the rGO. It is found that an apt rGO ratio in nanocomposite leads to a noticeable positively shifted valence band edge potential, meaning an increased oxidation power. The tunable band structure of the CN/rGO nanocomposites can be ascribed to the formation of C−O−C covalent bonding between the rGO and g-C_3N_4 layers, which has been experimentally confirmed by Fourier transform infrared (FT-IR) and X-ray

photoelectron (XPS) data. The resulting nanocomposites as photocatalysts have been evaluated by photocatalytic degradation of rhodamine B (RhB) and 4-nitrophenol under visible light irradiation (λ>400 nm). The results demonstrate that the photocatalytic activities of the CN/rGO nanocomposites are strongly influenced by rGO ratio. With an apt rGO ratio of 2.5%, the CN/rGO-2.5% nanocomposite exhibits the highest photocatalytic efficiency, which is almost 3.0 and 2.7 times of the pure g-C_3N_4 toward photocatalytic degradation of RhB and 4-nitrophenol, respectively. This improved photocatalytic activity could be attributed to the improved visible light utilization, oxidation power and electron transport property due to the significantly narrowed bandgap, positively shifted valence band edge potential, and enhanced electronic conductivity.

1. Introduction

Graphitic carbon nitride (g-C_3N_4) has become an attractive candidate as visible light photocatalyst due to its excellent sunlight harvesting capability, superior physicochemical and photochemical stabilities, plentiful material source and inexpensive to synthesize.[1] In comparison with other g-C_3N_4 allotropes, the small bandgap (*ca.* 2.70 eV) of g-C_3N_4 is a result of the sp^2 hybridization of the carbon and nitrogen that form the π-conjugated graphitic planes, having comparable graphite structure.[1, 2] It is well known that the materials with delocalized conjugated π structure have been confirmed to have high charge separation efficiency and low charge recombination rate. However, the obtained visible light photocatalytic activity of pure g-C_3N_4 is rather low due to the marginal visible light absorption and grain boundary effects.[3] Moreover, the weak van der Waals interaction between adjacent conjugated planes also limits the electron coupling between the planes that negatively affect the electron transfer and photocatalytic activity.[4] Aiming to improve the

visible light photocatalytic efficiency of the g-C_3N_4-based photocatalyst, a new strategy of compositing g-C_3N_4 with other semiconductors has been widely investigated.[5, 6]

As the thinnest material, graphene has received considerable attention due to its unique optical, electronic and mechanical properties, promising for a range of applications such as solar energy conversion, photocatalysis, sensing and fuel cells.[7-13] Graphene and g-C_3N_4 possess similar carbon network and sp^2 conjugated π structure, which make them the most compatible materials to form composites. Importantly, the resultant composites should possess an enhanced photocatalytic activity because the superior electronic properties introduced by the graphene component facilitating electron transfer and charge separation processes. Quan's group recently reported a graphene oxide modified g-C_3N_4 composite fabricated via a sonochemical approach that demonstrated a visible light photocatalytic activity toward the degradation of rhodamine B and 2, 4-dichlorophenol.[14] Instead of graphene oxide, Zhang and co-workers used rGO to form non-covalently composite with g-C_3N_4, leading to an enhanced optoelectronic conversion property.[3] However, their work did not provide information regarding the actual weight ratio of g-C_3N_4 to rGO in the resultant nanocomposite. Moreover, in their study, the bandgap of the fabricated composite was found to be almost constant with different rGO to g-C_3N_4 ratios. Generally, for a composite semiconductor photocatalyst containing rGO, the altered band structure originated from the composited rGO is responsible for the enhanced visible light photocatalytic activity as demonstrated by a number of reports where they use the rGO to narrow the photocatalyst bandgap to achieve high photocatalytic activities under visible light irradiation.[15-17]

Herein, we report a thermal conversion method to fabricate high visible light active g-C_3N_4/rGO (CN/rGO) nanocomposites formed by cross-linked approach. The band structure of the resulting nanocomposite can be readily tuned by simply controlling the weight ratio of cyanamide to graphene oxide (GO) in precursor materials. The conduction and valence band

positions of the obtained nanocomposites with different CN/rGO weight ratios have been investigated in detail using optical and electrochemical techniques. The fabricated CN/rGO nanocomposites with different band structures as photocatalysts have been systematically evaluated for photocatalytic degradation of rhodamine B (RhB) and 4-nitrophenol under visible light irradiation (λ>400 nm).

2. Results and Discussion

2.1 Structure and Morphology

CN/rGO nanocomposites with different rGO ratios were obtained by thermally treating the precursor materials consisted of cyanamide and GO with different weight ratios at 550 ºC for 4.0 h in Ar. **Table 1** summarizes the reaction condition, mass product yield, and composition of the fabricated nanocomposites with different weight ratios of rGO to g-C_3N_4. It was found that an increase in the added amount of GO in the reaction solution results in an slight increase in the product yield. The weight ratios of rGO to g-C_3N_4 in nanocomposites were estimated based on the product yield by assuming that the rGO weight in the nanocomposite equals the initial GO amount. The resultant nanocomposites are denoted as CN/rGO-x% (x% is the weight ratio of rGO to g-C_3N_4 in the nanocomposite). **Figure 1**a shows the photographs of pure g-C_3N_4 and CN/rGO nanocomposites. As shown, the color of the pure g-C_3N_4 is bright yellow. With increasing rGO ratio, the color of the resulting nanocomposites changes from slight gray for CN/rGO-1.6%, gray for CN/rGO-5.1% to dark gray for CN/rGO-19.6%. A similar phenomenon has also been observed for other carbon/semiconductor composite materials.[18-20] Figure 1b shows the X-ray diffraction (XRD) patterns of the pure g-C_3N_4, rGO and CN/rGO nanocomposites with different rGO ratios. As shown, a broad diffraction peak at around 24.3º was observed for the rGO, meaning that the rGO sheets were loosely stacked.[21] However, both of the pure g-C_3N_4 and CN/rGO nanocomposites show a strong characteristic (002) peak at 27.4º, corresponding to the interlayer-stacking of the conjugated aromatic

system with a stacking distance of 0.326 nm, indicating that the formed nanocomposites possess layered structures. The peak at 13.0º corresponding to *d* value of 0.676 nm is related to the in-plane ordering of tri-s-triazine units.[22] It was also found that with increasing rGO ratio in nanocomposites, the relative intensity of (002) peak increased. This could be due to an increase in structural correlation length introduced by large size rGO sheets.[23] Figures 1c and d show the transmission electronic microscopy (TEM) images of the pure g-C_3N_4 and CN/rGO nanocomposite (take CN/rGO-2.5% as an example). As shown, the TEM images clearly show the g-C_3N_4 and CN/rGO-2.5% with the lamellar structures. The TEM image of the pure g-C_3N_4 also indicates that numerous mesoporous structures with several tens of nanometres exist in the layers which are folded at the edges of the sample. For the CN/rGO-2.5%, it exhibits platelet-like textures similar with the pure g-C_3N_4 but forming multiple corrugated layers buckled together. The similar SAED patterns (insets in Figures 1c and d) of the pure g-C_3N_4 and CN/rGO-2.5% demonstrate the homogeneous distribution of monolayer rGO sheets in the layered g-C_3N_4 structure, implying an ignorable effect of rGO modification on the layered structure of g-C_3N_4. This can be supported by similar XRD patterns of the pure g-C_3N_4 and CN/rGO-2.5%.

2.2 Optical Property

UV-Vis diffuse reflectance spectra of the pure g-C_3N_4, rGO, and CN/rGO nanocomposites are shown in **Figure 2**a. Clearly, rGO modification importantly affects the optical property of the CN/rGO nanocomposites. As shown, all investigated samples exhibit strong visible light absorption. Moreover, with increasing rGO ratio in CN/rGO nanocomposite, a red shift to a longer wavelength was observed in the absorption edge of nanocomposite. Importantly, the red shift of the absorption band edge means the bandgap narrowing of the CN/rGO nanocomposite.[15, 24] Figure 2b shows the plots of the transformed Kubelka-Munk function as a function of light energy of all investigated samples. Based on Figure 2, the estimated

bandgaps are 2.50, 2.40, 2.34, 2.23 and 1.55 eV, corresponding to pure g-C_3N_4, CN/rGO-1.6%, CN/rGO-2.5%, CN/rGO-5.1% and CN/rGO-19.6%, respectively. This supports the observation of a red shift in the absorption band edge of CN/rGO nanocomposite as compared to the pure g-C_3N_4. Similar phenomenon has also been observed in the case of the TiO_2/rGO composite materials, which can be attributed to the formation of the chemical bonding between TiO_2 and the specific sites of rGO (e.g., Ti−O−C bonding) that can form localized occupied states in the bandgap of TiO_2, leading to a red shift of the absorption band edge, as reported by other groups.[15, 25] In the case of CN/rGO nanocomposites in our work, the reason of the bandgap narrowing has never been addressed in literatures. However, similar to the TiO_2/rGO composite, the oxygen-rich active sites on the GO surface (e.g., −OH, −COOH) can play key role of cross-linkers to form C−O−C covalent bonding between rGO and g-C_3N_4 during thermal conversion, which could be the reason for the bandgap narrowing and enhanced visible light absorption of the nanocomposites.[26] The above results imply that the combination of rGO with g-C_3N_4 is not simply through π-π stacking interaction.[3] Recently, Afroze et al. found that C−O−C covalent bonding can be easily formed owing to oxygen rearrangement under high temperature through thermal treatment of plasma polymerized 1, 1, 3, 3-tetramethoxy-propane (PPTMP) thin films.[26] The formation of C−O−C covalent bonding results in a red shift in the absorption band edge of the resulting material.[26] Further, theoretical calculations illustrated that oxygen near the conduction and valence bands originated from the C−O−C covalent bonding which introduces extra *p* states can also decrease the bandgap of a semiconductor.[27] It can be also seen from Figure 2a that the rGO modification in g-C_3N_4 can not only narrow the bandgap of the nanocomposite, but also improve visible light utilization (stronger absorption intensity of the CN/rGO nanocomposites than that of the pure g-C_3N_4), which can be advantageous to enhancing the visible light photocatalytic activity of the nanocomposite. However, too high rGO ratio in nanocomposite

is also disadvantageous because most of the incident light will be absorbed by rGO, resulting in a decreased light utilization of g-C_3N_4. Therefore, an apt rGO ratio in nanocomposite could be critically important for improving the light utilization, thus photocatalytic efficiency. It is well known that photoluminescence (PL) analysis is usually used to investigate the carrier separation efficiency of semiconductor photocatalyst.[28] Figure 2c shows the PL spectra of pure g-C_3N_4, rGO, and CN/rGO nanocomposites. As shown, the PL spectrum of the pure g-C_3N_4 shows a strong PL emission band at 450 nm that is equivalent to 2.7 eV. This strong peak can be attributed to the band-band PL phenomenon, resulting from the n-π* electronic transitions in g-C_3N_4.[29] Apparently, rGO modification leads to significant fluorescence quenching of the CN/rGO nanocomposites. Moreover, the extent of the fluorescence quenching was found to be noticeably increased with increasing rGO ratio, indicating a decreased recombination of photogenerated electrons and holes in nanocomposites because rGO acting as an electron collector. Overall, an apt rGO ratio could significantly improve the photogenerated carrier separation efficiency, thus enhancing light utilization and photocatalytic efficiency.

It is well known that the performance of semiconductor photocatalysts is highly dependent on their band structures.[30] To further investigate the effect of rGO ratio on the band structure of the CN/rGO nanocomposite, the flat band potentials (E_{fb}) of the CN/rGO nanocomposites have been measured by electrochemical technique, which can be used to approximately estimate the conduction band edge potentials (E_{cb}) of the CN/rGO nanocomposites.[31] **Figure 3**a shows the Mott-Sckottky plots of pure g-C_3N_4 and CN/rGO nanocomposites with different rGO ratio in dark, revealing typical n-type characteristics for these CN/rGO nanocomposites.[32] The E_{cb} potentials derived from Mott-Schottky plots are about -1.27,-1.16, -0.96, -0.95 and -0.74 V for pure g-C_3N_4, CN/rGO-1.6%, CN/rGO-2.5%, CN/rGO-5.1% and CN/rGO-19.6%, respectively (Figure 3b). Obviously, the conduction band edge potentials of

the CN/rGO nanocomposites occur to positive-shift compared to pure g-C_3N_4, and CN/rGO-19.6% exhibits the biggest positive-shift of E_{cb}. Based on the bandgap data of the nanocomposites obtained by UV-vis diffuse reflectance spectra (Figure 2a), the calculated valence band potentials (E_{vb}) for all investigated photocatalysts are *ca*. 1.23, 1.24, 1.38, 1.28 and 0.81 V for pure g-C_3N_4, CN/rGO-1.6%, CN/rGO-2.5%, CN/rGO-5.1% and CN/rGO-19.6%, respectively, as shown in Figure 3b. Compared to pure g-C_3N_4, the E_{vb} of the CN/rGO-1.6%, CN/rGO-2.5% and CN/rGO-5.1% apparently happens to positive-shift, while a negative-shift of E_{vb} occurs for the CN/rGO-19.6%. Among all samples, the CN/rGO-2.5% displays the most positive valence band potential, meaning higher oxidation power in comparison with other samples. The above results indicate that an apt rGO ratio can significantly adjust the band structure of the nanocomposite, and thus the photocatalytic efficiency.

Figure 4 shows the FT-IR spectra of GO, rGO, pure g-C_3N_4 and CN/rGO nanocomposites. The FT-IR spectrum of GO shows C=O (1725 cm^{-1}), aromatic C=C (1621 cm^{-1}), carboxyl C−O (1382 cm^{-1}), epoxide/ether C−O−C (1231 cm^{-1}), and alkoxy/alkoxide C−OH stretches (1027 cm^{-1}).[33] However, almost all of these non-sp^2 carbon bonds are disappeared after thermal treatment at 550 °C, indicating GO reduction to form rGO.[34] It is known for GO that carboxylic and lactone groups begin to decompose at ~250 °C, and −COOH and carbonyl groups are reduced at *ca*. 450 °C.[35] Phenol and quinone groups decompose almost entirely between 500 and 900 °C. Above 900 °C, −OH groups start to decrease and oxygen-containing groups in GO are completely eliminated at ~1100 °C.[35] As shown in Figure 4, except for −OH group, almost all of other oxygen-containing functional groups on the GO surface were removed at 550 °C (see the rGO curve in Figure 4), which means that the non-removed –OH groups could act as cross linkers to connect rGO and g-C_3N_4 by forming C−O−C bonds in the nanocomposites during thermal conversion. Obviously, the C−O−C peak at ~1231 cm^{-1} can

be observed for all investigated CN/rGO nanocomposites (Figure 4), further indicating that the non-removed –OH groups on the rGO surface can be used as cross linkers to link rGO and g-C_3N_4, resulting in bandgap narrowing of the nanocomposite.[27]

X-ray photoelectron spectroscopy (XPS) technique was further employed to characterize the elemental composition and oxygen bonding configurations in CN/rGO nanocomposites. As shown in **Figure 5**a, the XPS survey spectra of pure g-C_3N_4 shows only carbon and nitrogen elements. However, the CN/rGO nanocomposite (take CN/rGO-2.5% as an example) clearly shows the presence of carbon, nitrogen and oxygen elements, indicating the incorporation of oxygen into the framework of CN/rGO nanocomposite (Figure 5a). Similar results can be also obtained for other CN/rGO nanocomposites. The O/C atomic ratio is calculated to be around 0.095 for CN/rGO-2.5%. It is also found that oxygen content in CN/rGO nanocomposites can be tuned by simply controlling the GO ratio in reaction precursors (e.g., O/C atomic ratio of 0.55 for CN/rGO-19.6%). Figure 5b shows the high resolution C1s XPS spectra of pure g-C_3N_4. As shown, three fitted peaks at 284.8, 286.9 and 287.8 eV can be observed. The peaks located at about 284.8 and 286.9 eV are corresponding to bulk graphitic sites in a CN matrix and sp^2 C bonded to N in an aromatic ring.[36] Moreover, the smaller peak centred at 284.8 eV also illustrates that the pure g-C_3N_4 has a lower graphitic degree, meaning low conductivity.[37] The peak located at 287.8 eV is corresponding to sp^3-bonded C in C−N. [36] Different from the pure g-C_3N_4, the C1s XPS spectra of CN/rGO-2.5% exhibits a new peak at ~287.5 eV, which is attributed to the formation of C−O−C bonding configurations during thermal treatment (Figure 5d),[38] and the high resolution O1s XPS spectra of CN/rGO-2.5% further confirms the presence of oxygen in the nanocomposite (Figure 5f).

Similarly, the bonding configurations of nitrogen atoms in g-C_3N_4 (Figure 5c) and CN/rGO-2.5% (Figure 5e) were also investigated by high resolution N1s XPS spectra. The

N1s XPS spectra of pure g-C_3N_4 and CN/rGO-2.5% can be fitted into three peaks centred at 398.3, 399.5, and 400.2 eV, respectively. The peaks with lower binding energy located at about 398.2 and 399.5 eV, corresponding to pyridinic-like (N-sp^2C) and pyrrolic like (N-sp^3C) nitrogen, respectively, while the peak centred at 400.2 eV corresponds to graphitic nitrogen.[39] Further, the peak at 399.5 eV corresponding to N-sp^3C confirms the formation of g-C_3N_4, which is in agreement with the XRD results of pure g-C_3N_4.[39] Based on the above investigations, some conclusions can be drawn that most of oxygen functional groups in GO can be removed at 550 °C. However, the non-removed −OH groups during thermal treatment can act as the cross-linker role for forming C−O−C bonds responsible for the narrowed bandgap of the nanocomposites (**Figure 6**).

2.3 Photocatalytic Evaluation

Owing to excellent visible light activity, g-C_3N_4 based photocatalysts have been widely investigated for environmental remediation and photocatalytic production of hydrogen.[5, 6, 22] In this work, the fabricated CN/rGO nanocomposites with tunable band structures as photocatalysts were evaluated by photocatalytic degradation of rhodamine B (RhB) and 4-nitrophenol under visible light irradiation (λ>400 nm). For comparison, pure g-C_3N_4 was also measured. Prior to light irradiation, 5.0 mg/L RhB (or 10 mg/L 4-nitrophenol) solutions containing photocatalysts were maintained in dark for 0.5 h to achieve adsorption equilibrium. **Figure 7**a shows the photocatalytic degradation curves of RhB with light irradiation time for different photocatalysts. As shown, under visible light irradiation (λ>400 nm), no noticeable degradation of RhB (curve a) was observed with direct photolysis without photocatalyst. Without visible light irradiation, no degradation of RhB can be observed in the presence of CN/rGO photocatalyst (take CN/rGO-2.5% as an example, curve b). Under visible light irradiation, it was found that the degradation efficiency of RhB initially increases, then decreases with increasing rGO ratio in CN/rGO nanocomposites. The best degradation

efficiency was obtained with CN/rGO-2.5% photocatalyst (curve i), as shown in Figure 7a. After 75 min of visible light irradiation, 84%, 100%, 52%, 36% and 80% of RhB were degraded using CN/rGO-1.6%, CN/rGO-2.5%, CN/rGO-5.1%, CN/rGO-19.6%, and pure g-C_3N_4, respectively. Obviously, an apt rGO ratio in CN/rGO nanocomposite (e.g., rGO ratio of 2.5% in nanocomposite) can significantly improve the resulting photocatalytic activity compared to pure g-C_3N_4. This improved photocatalytic activity of the nanocomposite with an apt rGO ratio could be due to some advantages: (1) narrowed bandgap of the nanocomposite, responsible for the improved visible light utilization; (2) very positive valence band potential, resulting in high oxidation power of the nanocomposite; (3) superior electron transport property owing to rGO acting as electron collectors, and therefore decreasing the charge recombination. These advantages of rGO in nanocomposites can dramatically increase their photocatalytic performance. However, the nanocomposites with too high rGO ratio (e.g., CN/rGO-5.1% and CN/rGO-19.6%) will be disadvantageous for improving the photocatalytic activity because most of incident visible light will be absorbed by rGO, resulting a decreased light utilization of g-C_3N_4. Therefore, an apt rGO ratio in nanocomposite is critically significance for improving the resultant photocatalytic performance. Also, using all investigated photocatalysts, it was found that the photocatalytic degradation of RhB follows first-order reaction dynamics under our experimental conditions. Based on the first-order equation:

$$\ln(\frac{C_0}{C_t}) = Kt$$

where k is the rate constant (min^{-1}), C_0 is the initial concentration of RhB, and C_t is the actual concentration of RhB at time t. The linear relationships between ln (C_0/C_t) and the light irradiation time of the photocatalysts are given in Figure 7b. As shown, the photocatalytic degradation rate of CN/rGO-2.5% toward RhB is almost 3.0 times of pure g-C_3N_4, and 2.3, 6.8 and 11.3 times of CN/rGO-1.6%, CN/rGO-5.1% and CN/rGO-19.6% under the same

experimental conditions, respectively. Apparently, CN/rGO-2.5% displays the best photocatalytic activity toward RhB degradation among all investigated photocatalysts. Further, the photocatalytic degradation mechanisms of RhB using CN/rGO nanocomposites were also investigated in this work. CN/rGO-2.5% was chose to use as photocatalyst for this purpose. As we know, the triethanolamine (TEOA) is an effective hole scavenger for photocatalytic reaction.[5] In this work, it was found that the photocatalytic degradation efficiency significantly decreased when 10 vol% TEOA was introduced into the reaction system (curve c in Figure 7a). However, TBA (a radical scavenger) was added to the reaction solution, the photocatalytic degradation was hardly suppressed (curve h in Figure 7a). The above experimental results indicate that the photocatalytic degradation of RhB using CN/rGO nanocomposite can be due to a direct photoholes oxidation under visible light irradiation.

It is worth pointing out that the stability of a given photocatalyst during photocatalytic reaction is a crucial factor for its practical application. Stability tests were therefore evaluated by carrying out repeatedly photocatalytic reaction using CN/rGO-2.5% photocatalyst under visible light irradiation. The results demonstrate that after repeating use of five times, only 1.1% decrease in photocatalytic degradation efficiency can be achieved, indicating a high stability of the fabricated CN/rGO photocatalyst, as shown in Figure 7c.

In this work, the photocatalytic degradation of 4-nitrophenol was also performed using the fabricated photocatalysts. As shown in Figure 7d, the CN/rGO-2.5% exhibits the best photocatalytic activity toward photocatalytic degradation of 4-nitrophenol, which is almost 2.7, 2.0, 3.5 and 4.3 times of g-C_3N_4, CN/rGO-1.6%, CN/rGO-5.1% and CN/rGO-19.6%, respectively, after 150 min of visible light irradiation. When TEOA (10 vol%) was added into the reaction system, only 0.8% 4-nitrophenol was degraded, which further proved the photocatalytic degradation was due to a direct photohole oxidation under visible light

irradiation. The above results further confirm that the fabricated CN/rGO nanocomposite with an apt rGO ratio possesses excellent visible light activity.

3. Conclusions

In summary, we have successfully prepared the g-C_3N_4/rGO (CN/rGO) nanocomposites with different rGO ratios by a facile thermal conversion method. It was found that the CN/rGO nanocomposites were formed by cross-linked C−O−C bonds during thermal conversion. The influence of rGO ratio on the resulting photocatalytic activity of CN/rGO nanocomposites has been investigated in detail by photocatalytic degradation of RhB and 4-nitrophenol under visible light irradiation. It was found that CN/rGO-2.5% exhibited the best photocatalytic activity toward photocatalytic degradation of RhB and 4-nitrophenol. This importantly improved photocatalytic activity of the nanocomposite is mainly due to an apt rGO ratio resulting in improved light utilization, high oxidation capability, and superior electron transport property ascribing to narrowed bandgap, positively shifted valence band edge potential, and enhanced electronic conductivity, respectively. The approach used in this work can be extended to synthesize other rGO modified semiconductor materials for applications in photocatalysis, solar energy conversion and fuel cells.

4. Experimental Section

Chemicals: Natural graphite powder (325 meshes) was purchased from Chem Supply (Australia), and all of other reagents with analytical grade purity were purchased from Sigma Aldrich and used without further purification.

Preparation of graphene oxide (GO): Graphene oxide was synthesized by modified Hummers method through oxidation of graphite powder. [40, 41] Typically, the graphite powder (5.0 g) was added into an 80 ºC solution composed of concentrated H_2SO_4 (30 ml), $K_2S_2O_8$ (3.0 g) and P_2O_5 (3.0 g), and then reacted for 6.0 h. The resultant dark blue mixture was cooled down to room temperature, then washed adequately with distilled water until pH of the

filtrate was close to 7.0 and dried in an oven at 80 ºC overnight. Then, 2.5 g of pre-oxidized graphite was placed into 115 mL of cold (0 ºC) concentrated H_2SO_4 solution. $KMnO_4$ (7.5 g) was added gradually into the above solution under stirring, and the temperature of the mixture was kept below 20 ºC for 2.0 h. The mixture was then stirred at 35 ºC for 3.5 h. After that, 230 mL of water was slowly added into the above mixture, and then reacted for another 1.5 h at room temperature. More water (300 ml) and 30% H_2O_2 (6.5 ml) were then added into the above solution to terminate the reaction. The mixture was subsequently washed with diluted HCl solution and centrifuged. The resulting product was further washed and dialyzed for one week.

Preparation of g-C_3N_4 and rGO modified g-C_3N_4 (CN/rGO) nanocomposites: GO aqueous solution (1.0 mg/mL) was mixed with cyanamide (99%, Sigma Aldrich) with different weight ratios, and then was concentrated into a paste at 100 ºC on a hot plate. After that, the synthesized product was grinded into fine powders and put into a crucible, and then heated to 550 ºC for 4.0 h in Ar atmosphere. Pure g-C_3N_4 was prepared by heating only cyanamide under the same preparation conditions as CN/rGO nanocomposites. The rGO modified g-C_3N_4 nanocomposite was denoted as CN/rGO-x%, where x% is the initial weight ratio of GO to cyanamide.

Characterization: TEM (Philips F20) and XRD (Shimadzu XRD-6000 diffractometer, equipped with a graphite monochromator) were employed for characterising the sample structure. Chemical compositions of the samples were analysed by X-ray photoelectron spectroscopy (Kratos Axis ULTRA incorporating a 165 mm hemispherical electron energy analyzer). All binding energies were carefully aligned by reference to the C1s peak (284.6 eV) arising from surface hydrocarbons or possible adventitious hydrocarbon. UV-Vis diffuse reflectance spectra of the nanocomposites were recorded on a Varian Cary 5E UV-Vis-NIR spectrophotometer. Fourier transform infrared spectroscopy (FT-IR) analysis of the samples

was performed using Perkin Elmer spectrum 1000 FT-IR spectrophotometer with KBr as the reference sample. Photoluminescence spectra (PL) of the samples were obtained using a fluorescence spectrometer (Hitachi F-7000) at 293 K. The excitation wavelength was 315 nm, the scanning rate was 1200 nm/min, and the PMT voltage was 700 V. The widths of the excitation slit and emission slit were both 2.5 nm. Mott–Schottky curves were measured by a Princeton Applied Research PARSTAT 2273, using a three-electrode system.

Photocatalytic activity measurements: The photocatalytic activity was evaluated in a XPAII reactor (Nanjing Xujiang Machineelectronic Plant, China). The photocatalyst of 8.0 mg was put into 10 mL of quartz test tube containing 5.0 mL of 5.0 mg/L rhodamine B (RhB) and 10 mg/L 4-nitrophenol, and then stirred in dark for 0.5 h to achieve adsorption equilibrium before light irradiation. After that, a 1000 W Xe lamp (the UV light was cut off by 2.0 M sodium nitrite[42, 43]) was used as the visible light source to perform the photocatalytic experiment at 25 °C. The remaining concentration of RhB and 4-nitrophenol in reaction solution was determined using the UV-Vis spectrophotometer (UV-1800, Shimadu). The dispersion ability of the fabricated nanocomposites in aqueous medium is relatively low and the reaction solution was therefore constantly stirred during photocatalytic degradation process.

Acknowledgements

This work was finacially supported by Australian Research Council (ARC) Discovery Project.

[1] X. Wang, K. Maeda, A. Thomas, K. Takanabe, G. Xin, J. M. Carlsson, K. Domen, M. Antonietti, *Nat. Mater.* **2009,** *8*, 76.
[2] J. R. Holst, E. G. Gillan, *J. Am. Chem. Soc.* **2008,** *130*, 7373.
[3] Y. J. Zhang, T. Mori, L. Niu, J. H. Ye, *Energ. Environ. Sci.* **2011,** *4*, 4517.
[4] X. C. Wang, X. F. Chen, A. Thomas, X. Z. Fu, M. Antonietti, *Adv. Mater.* **2009,** *21*,1609.
[5] S. C. Yan, Z. S. Li, Z. G. Zou, *Langmuir.* **2010,** *26*, 3894.
[6] Y. J. Wang, R. Shi, J. Lin, Y. F. Zhu, *Energ. Environ. Sci.* **2011,** *4*, 2922.
[7] D. Li, M. B. Muller, S. Gilje, R. B. Kaner, G. G. Wallace, *Nat. Nano.* **2008,** *3*, 101-105.
[8] F. Schwierz, *Nat. Nano.* **2010,** *5*, 487.
[9] M. D. Stoller, S. Park, Y. Zhu, J. An, R. S. Ruoff, *Nano. Lett.* **2008,** *8*, 3498.
[10] I. V. Lightcap, T. H. Kosel, P. V. Kamat, *Nano. Lett.* **2010,** *10*, 577.
[11] E. Yoo, T. Okata, T. Akita, M. Kohyama, J. Nakamura, I. Honma, *Nano. Lett.* **2009,** *9*, 2255.
[12] I. Y. Kim, J. M. Lee, T. W. Kim, H. N. Kim, H.-i. Kim, W. Choi, S.-J. Hwang, *Small* **2012,** *8*, 1038.
[13] S. Y. Han, I. Y. Kim, K. Y. Jo, S.-J. Hwang, *J Phys Chem C* **2012,** *116*, 7269.
[14] G. Z. Liao, S. Chen, X. Quan, H. T. Yu, H. M. Zhao, *J. Mater. Chem.* **2012,** *22*, 2721.
[15] J. S. Lee, K. H. You, C. B. Park, *Adv. Mater.* **2012,** *24*, 1084.
[16] Y. J. Xu, Y. B. Zhuang, X. Z Fu, *J. Phys. Chem. C.* **2010,** *114*, 2669.
[17] K. Woan, G. Pyrgiotakis, W. Sigmund, *Adv. Mater.* **2009,** *21*, 2233.
[18] Q. Xiang, J. Yu, M. Jaroniec, *J. Phys. Chem. C.* **2011,** *115*, 7355.
[19] Y.J. Xu, Y. Zhuang, X. Fu, *J. Phys. Chem. C.* **2010,** *114*, 2669.
[20] J. Yu, T. Ma, S. Liu, *Phys. Chem. Chem. Phys.* **2011,** *13*, 3491.
[21] K. Zhang, L. L. Zhang, X. S. Zhao, J. Wu, *Chem. Mater.* **2010,** *22*, 1392.
[22] F. Dong, L. Wu, Y. Sun, M. Fu, Z. Wu, S. C. Lee, *J. Mater. Chem.* **2011,** *21*, 15171.
[23] F. Goettmann, A. Fischer, M. Antonietti, A. Thomas, *Angew. Chem. Int. Edit.* **2006,** *45*, 4467.
[24] H. M. Zhang, X. L. Liu,Y. B. Li, Q. F. Sun, Y. Wang, B. J. Wood, P. R. Liu, D. J. Yang, H. J. Zhao, *J. Mater. Chem.* **2012,** *22*, 2465.
[25] Di. Valentin, G. Pacchioni, A. Selloni, *Chem. Mater.* **2005,** *17*, 6656.
[26] T. Afroze, A. H. Bhuiyan, *Thin. Solid. Films.* **2011,** *519* (6), 1825-1830.
[27] A. Trejo, M. Calvino, E. Ramos, M. Cruz-Irisson, *Nanoscale. Res. Lett.* **2012,** *7*,7.
[28] L. K. van Vugt, S. J. Veen, E. P. A. M. Bakkers, A. L. Roest, D. Vanmaekelbergh, *J. Am.Chem. Soc.* **2005,** *127*, 12357.
[29] V. N. Khabashesku, J. L. Zimmerman, J. L. Margrave, *Chem. Mater.* **2000,** *12*, 3264.
[30] G. Liu, P. Niu, C. Sun, S. C. Smith, Z. Chen, G. Q. Lu, H.M. Cheng, *J. Am. Chem. Soc.* **2010,** *132*, 11642.
[31] K. Sayama, A. Nomura, T. Arai, T. Sugita, R. Abe, M. Yanagida, Y. Iwasaki, Y. Abe, H. Sugihara, *J. Phys. Chem.B.* **2006,** *110* , 11352.
[32] D.S. Kong, *Langmuir*.**2008,** *24*, 5324.
[33] V. Chandra, J. Park, Y. Chun, J. W. Lee, I.C. Hwang, K. S Kim, *Acs. Nano.* **2010,** *4*, 3979.
[34] D. Zangmeister, *Chem. Mater.* **2010,** *22*, 5625.
[35] X. Li, H. Wang, J. T. Robinson, H. Sanchez, G. Diankov, H. Dai, *J. Am. Chem. Soc.* **2009,** *131*, 15939.
[36] J. R. Shi, Y. J. Xu, J. Zhang, *Thin. Solid. Films.* **2005,** *483*, 169.
[37] A. B. Fuertes, T. A. Centeno, *J. Mater. Chem.* **2005,** *15*, 1079.
[38] H. Zhang, M. H. Harpster, H. J. Park, P. A. Johnson, W. C. Wilson, *Anal. Chem.* **2010,** *83*, 254.

[39] M. N. Uddin, Y. S Yang, *J. Mater. Chem.* **2009,** *19*, 2909.
[40] N. I. Kovtyukhova, P. J. Ollivier, B. R. Martin, T. E. Mallouk, S. A. Chizhik, E. V. Buzaneva, A. D. Gorchinskiy, *Chem. Mater.* **1999,** *11*, 771.
[41] W. S. Hummers, R. E. Offeman, *J. Am. Chem. Soc.* **1958,** *80*, 1339.
[42] J. Sun, J. Zhao, H. Guo, W. Wu, *Chem. Commun.* **2012,** *48*, 4169.
[43] X. Zhou, F. Peng, H. Wang, H. Yu, Y. Fang, *Chem. Commun.* **2011,** *47*, 10323.

Synopsis ToC Figure:

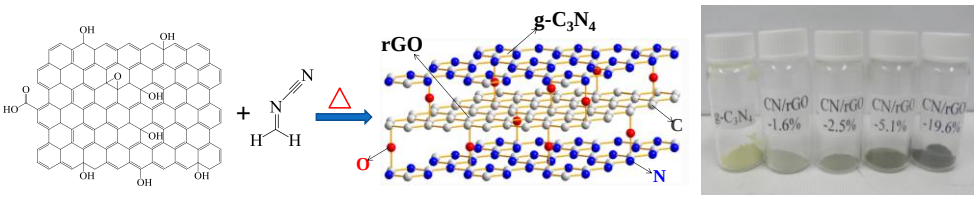

Tunable optical properties of the g-C_3N_4/reduced graphene oxide nanocomposite improve the visible light utilization, oxidation power and electron transport property, resulting in a dramatically enhanced visible light photocatalytic activity at the apt rGO ratio.

Table 1. Reaction condition, mass product yield and composition of the products

Samples	Reaction condition and mass product yield			Composition of the products			
	Cyanamide	GO solution (5ml)	Yield (%)	C (%)	N (%)	O (%)	Weight ratio of rGO to g-C_3N_4
g-C_3N_4	4000mg	0	9.62%	41.5%	58.5%	0	0
CN/rGO-1.6%	4000mg	6.4mg	9.90%	41.2%	56.3%	2.5%	1.6%
CN/rGO-2.5%	4000mg	10mg	10.0%	40.9%	55.2%	3.9%	2.5%
CN/rGO-5.1%	4000mg	20mg	10.4%	39.6%	52.9%	7.5%	5.1%
CN/rGO-19.6%	4000mg	80mg	11.9%	34.5%	46.6%	18.9%	19.6%

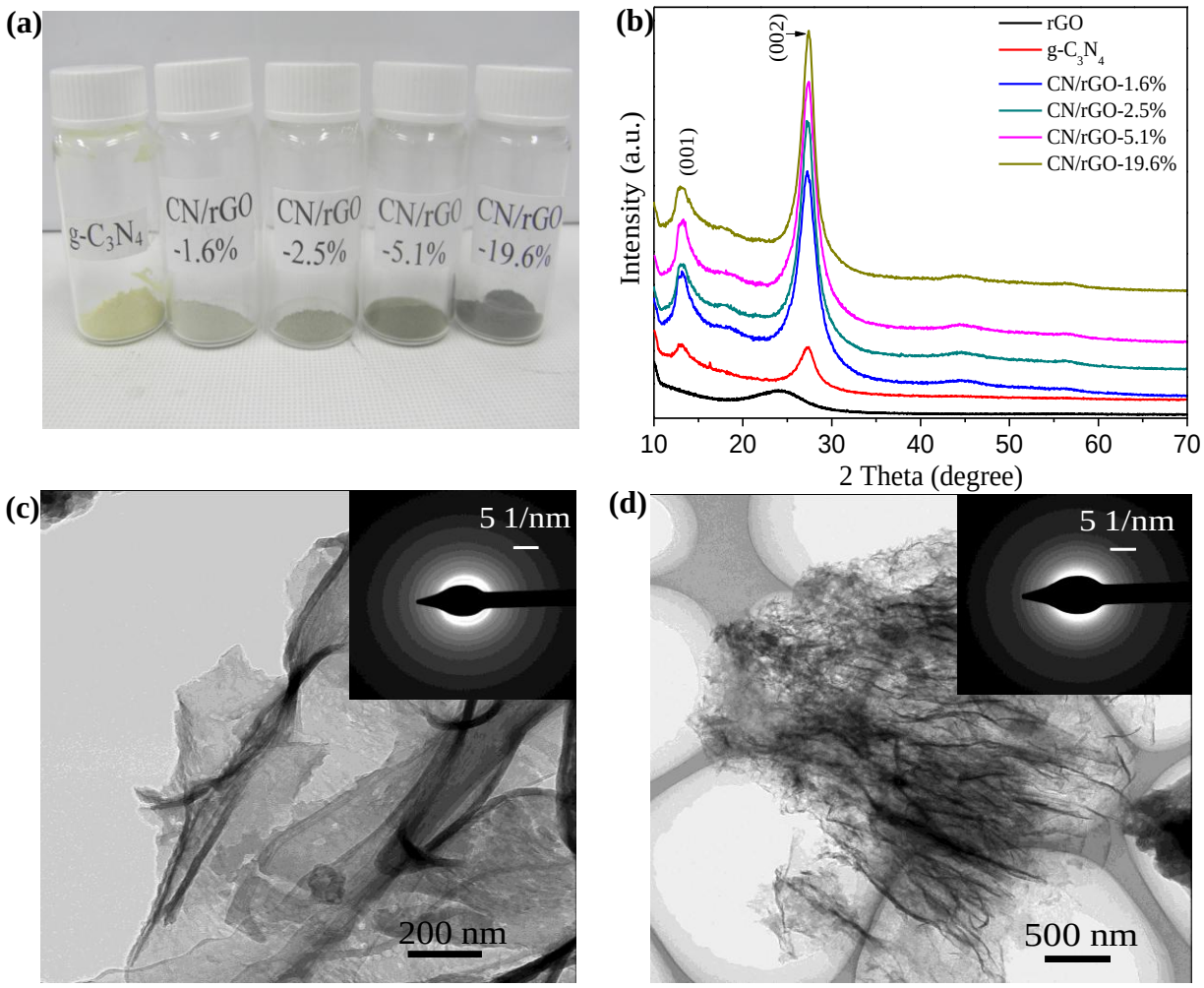

Figure 1. (a) Photographs of pure g-C_3N_4 and CN/rGO nanocomposites, in which, from left to right, weight ratio of rGO to g-C_3N_4 in the final product are 0.0%, 1.6%, 2.5%, 5.1% and 19.6%, respectively. (b) XRD patterns of the pure g-C_3N_4, rGO and CN/rGO nanocomposites; (c) and (d) TEM images and their corresponding SAED patterns (insets) of pure g-C_3N_4 and CN/rGO-2.5%, respectively.

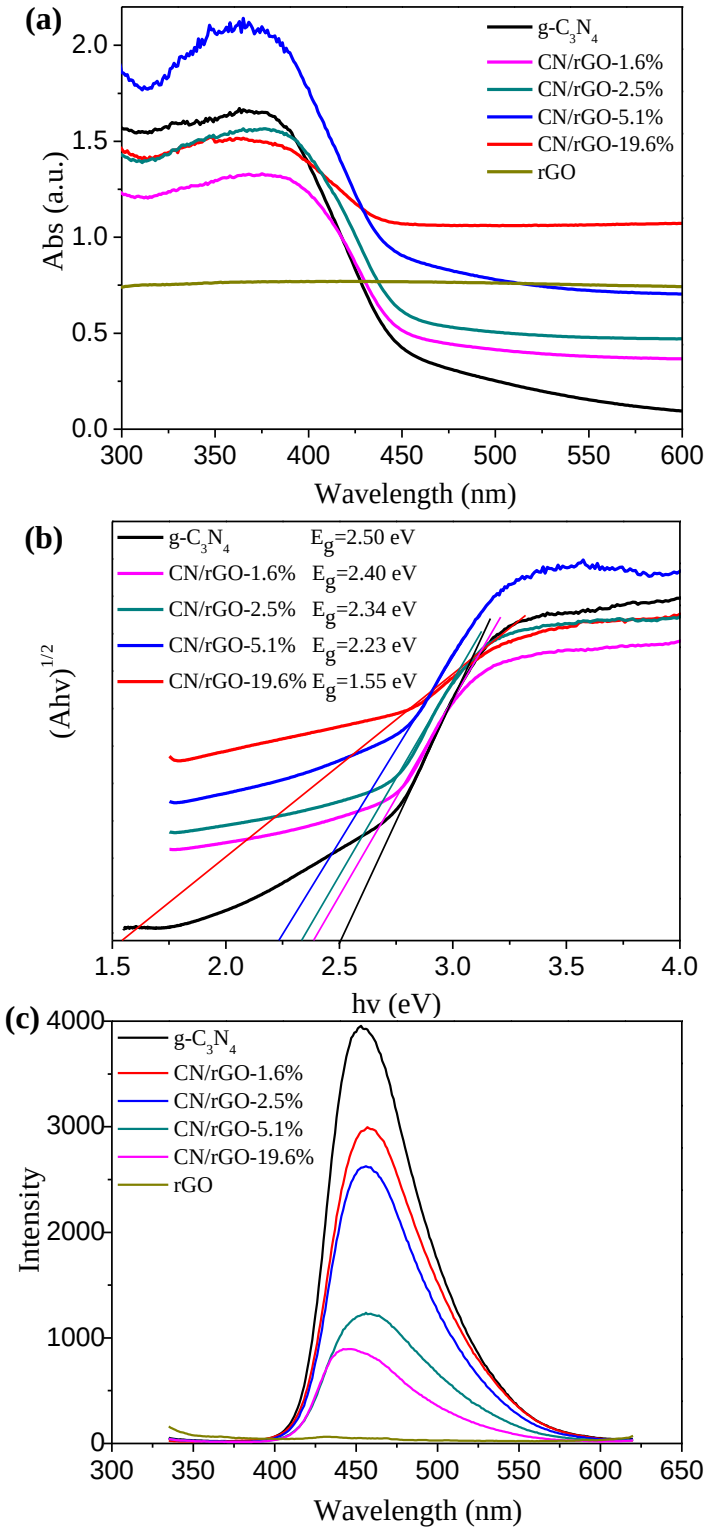

Figure 2. (a) UV-Vis diffuse reflectance spectra of the pure g-C_3N_4, rGO, and CN/rGO nanocomposites. (b) The plots of transformed Kubelka-Munk function versus the light energy. (c) Photoluminescence (PL) spectra of the g-C_3N_4, rGO, and CN/rGO nanocomposites.

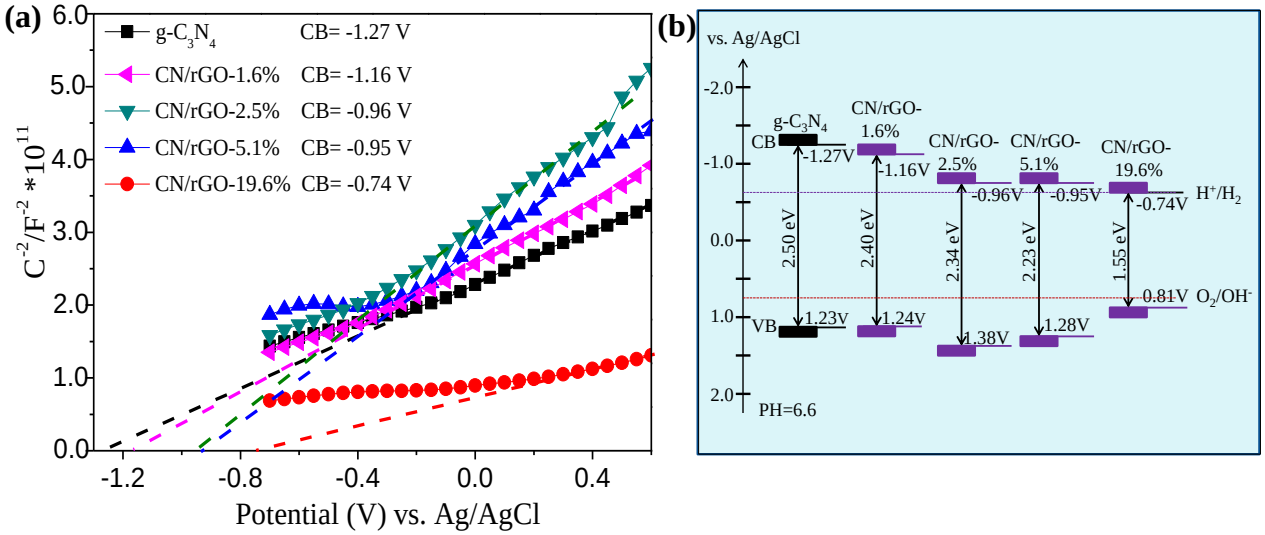

Figure 3. (a) Mott-Schottky plots of pure g-C_3N_4 and CN/rGO nanocomposites at a fixed frequency of 800 Hz. (b) Schematic illustration of band structures (CB: conduction band, VB: valence band) of pure g-C_3N_4 and CN/rGO nanocomposites.

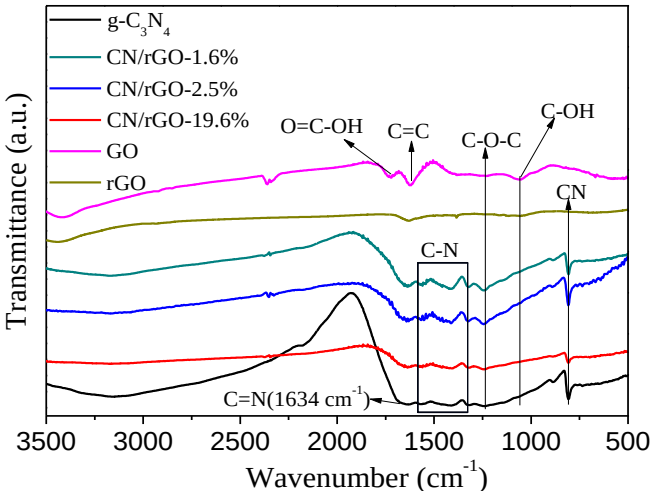

Figure 4. FT-IR spectra of GO, rGO, g-C_3N_4 and CN/rGO nanocomposites.

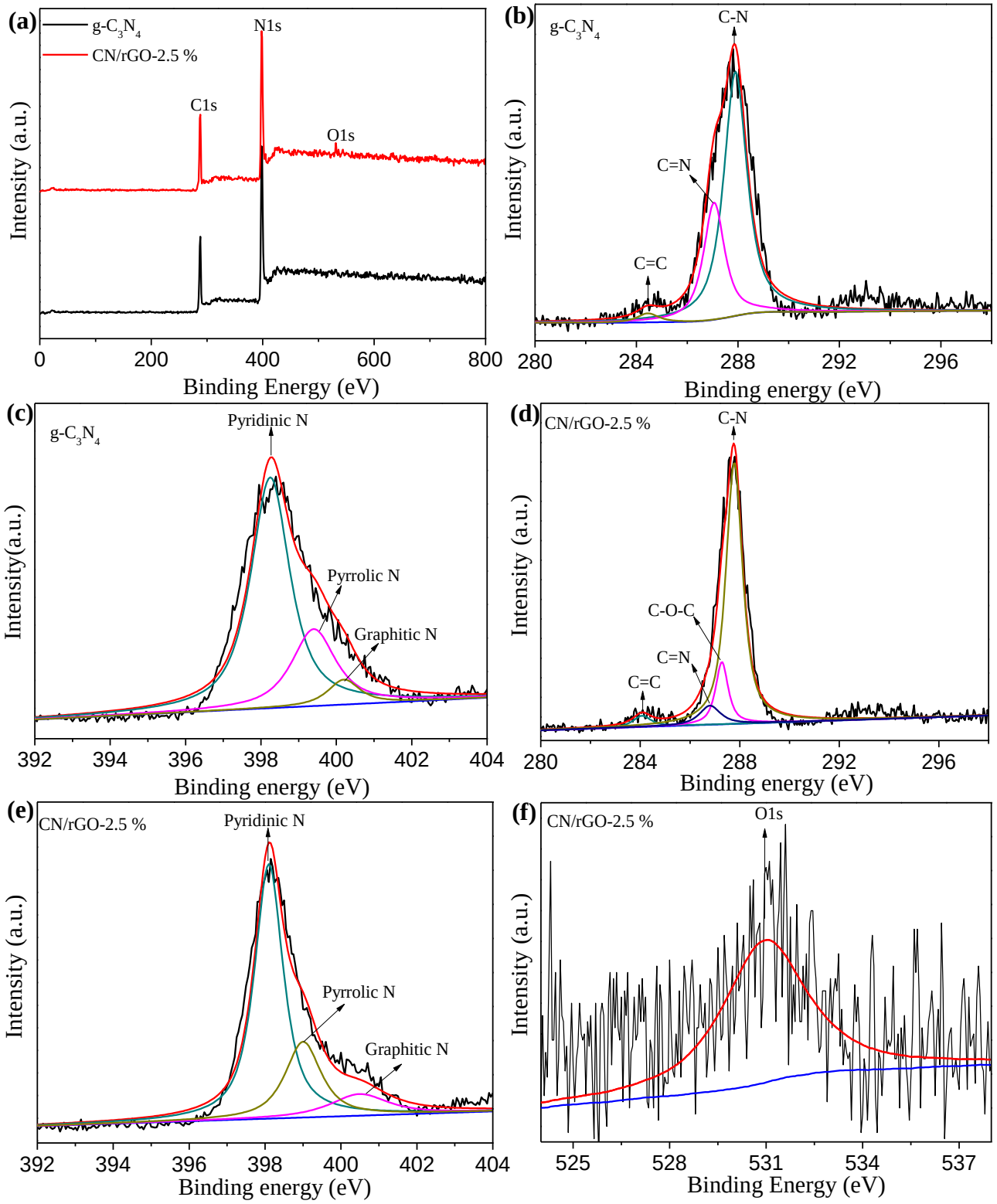

Figure 5. (a) XPS survey spectra of the synthesized g-C_3N_4 and CN/rGO-2.5% samples. High resolution C1s (b) and N1s (c) spectra of pure g-C_3N_4. High resolution C1s (d), N1s (e) and O1s (f) spectra of CN/rGO-2.5%.

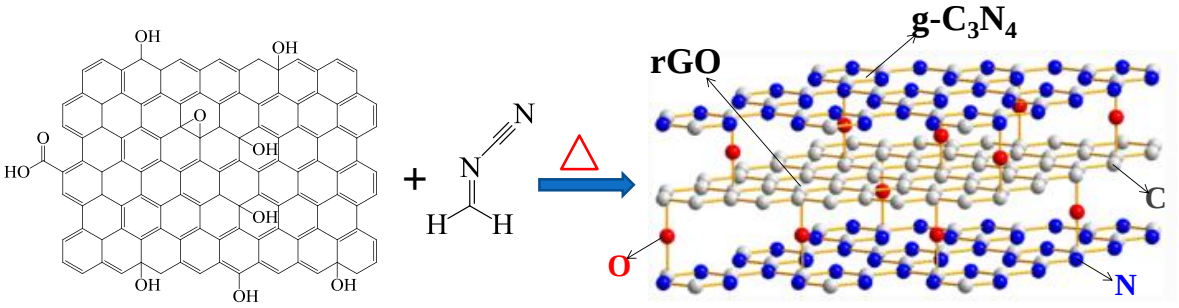

Figure 6. Schematic illustration of the reaction process and the CN/rGO nanocomposite structure. Gray, blue and red spheres represent carbon, nitrogen and oxygen atoms in CN/rGO, respectively.

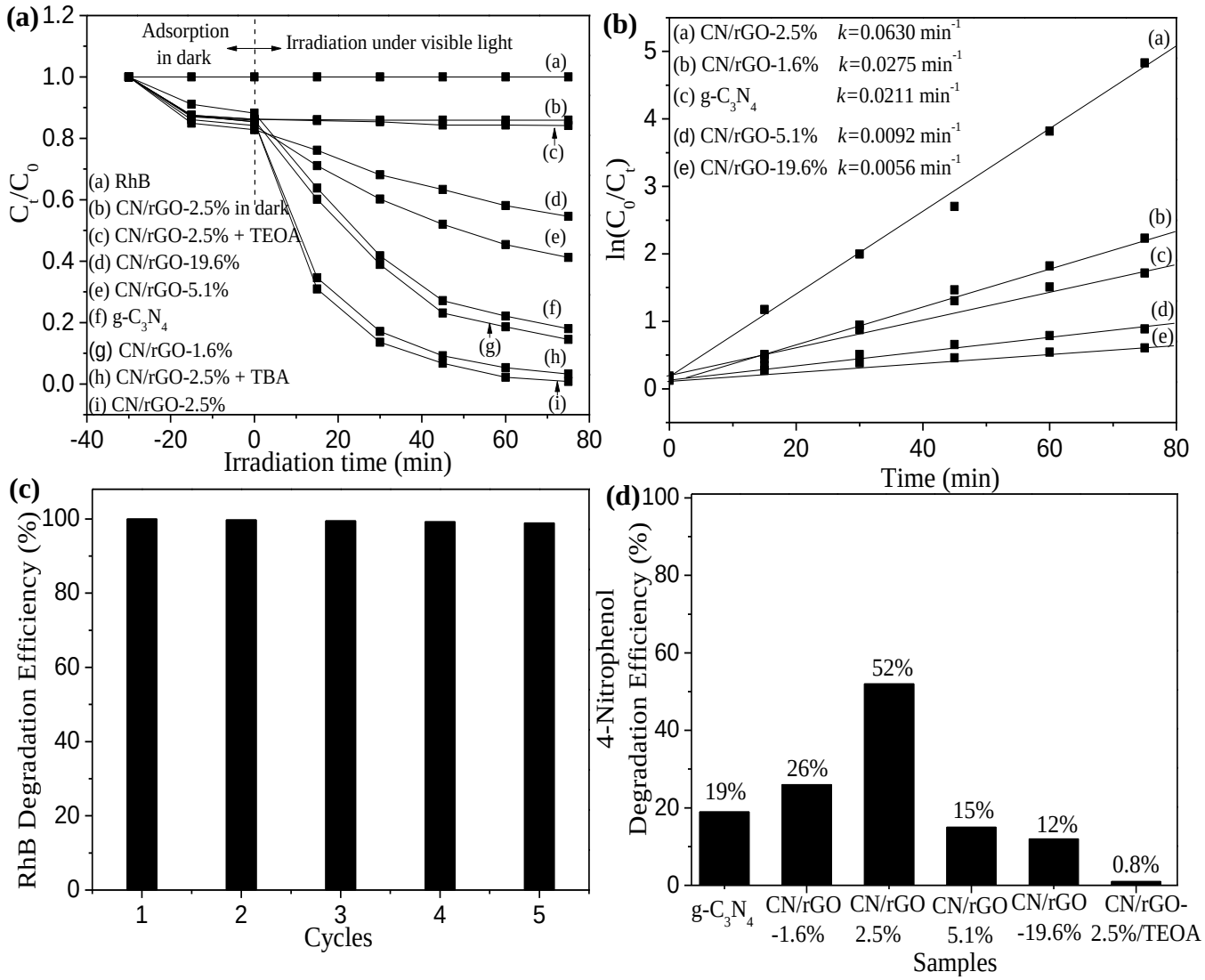

Figure 7. (a) Photocatalytic activities and (b) The degradation efficiency for the g-C_3N_4 and CN/rGO photocatalysis system. (c) Recycle test of CN/rGO-2.5% catalyst towards RhB degradation for 75 min and (d) Photocatalytic activities for the g-C_3N_4 and CN/rGO photocatalysis system towards 4-nitrophenol degradation for 150 min.